ACS OMEGA

http://pubs.acs.org/journal/acsodf

Article

# Pathways and Kinetics for Autocatalytic Reduction of $CO_2$ into Formic Acid with Fe under Hydrothermal Conditions

Binbin Jin, Ligang Luo,* and Longfei Xie

Cite This: *ACS Omega* 2021, 6, 11280−11285

Read Online

ACCESS | Metrics & More | Article Recommendations

**ABSTRACT:** The utilization of $CO_2$, as a cheap and abundant carbon source to produce useful chemicals or fuels, has been regarded as one of the promising ways to reduce $CO_2$ emissions and minimize the green-house effect. Previous studies have demonstrated that $CO_2$ (or $HCO_3^-$) can be efficiently reduced to formic acid with metal Fe under hydrothermal conditions without additional hydrogen and any catalyst. However, the pathways and kinetics of the autocatalytic $CO_2$ reduction remain unknown. In the present work, the reaction kinetics were carefully investigated according to the proposed reaction pathways, and a phenomenological kinetic model was developed for the first time. The results showed that the hydrothermal conversion of $HCO_3^-$ into formic acid with Fe can be expressed as the first-order reaction, and the activation energy of $HCO_3^-$ is 28 kJ/mol under hydrothermal conditions.

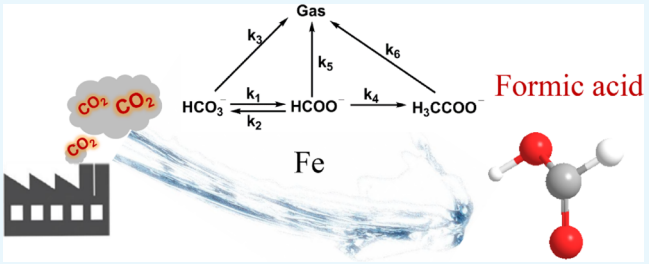


## 1. INTRODUCTION

Due to the increasing demand for energy and consumption of fossil fuels, the level of $CO_2$ atmosphere has raised at a faster rate, which leads to a series of problems in the environment and ecological balance.[1−3] In recent years, a great deal of focus has been expended to reduce the $CO_2$ concentration in the atmosphere, such as photosynthesis, electrochemical and biochemical technology, and so on.[4−7] Among these methods, artificial photosynthesis is regarded as one of the most promising methods for solar energy technologies.[8] However, there are still many challenges in the direct conversion of $CO_2$ using solar energy, such as the low conversion efficiency and product selectivity. Recently, the catalytic reduction of $CO_2$ with hydrogen has attracted increasing attention due to its commercial feasibility.[9−11] Nevertheless, high purity hydrogen and noble metal catalysts (Ir, Ru, Rh, etc.) are usually needed in the reduction process, leading to high energy consumption and cost.[12,13] Therefore, the development of an alternative method for the feasible reduction of $CO_2$ is highly desirable.

Hydrothermal chemistry has played an important role in the formation of fossil fuels and origin of life in the earth's crust and deep-sea hydrothermal vents.[14−16] The abiotic synthesis of organics suggests that highly efficient dissociation of $H_2O$ and the subsequent reduction of $CO_2$ into organics could be achieved with metals under hydrothermal conditions. In the abiotic synthesis of organics, the generally inferred pathway involves the reduction of $CO_2$ dissolved in water that accompanies the hydrothermal alteration of minerals, in which a primary role for the minerals is to generate $H_2$ through the reducing conditions as the reaction of ferrous Fe-bearing minerals with water.[17,18] Recently, Jin's group has developed a new strategy for the hydrothermal reduction of $CO_2$ with various zero-valent metals, such as Fe, Zn, and Mn, and it was found that formic acid was the main product from reduction of $CO_2$.[19−22] As an important chemical, formate can serve as the raw material for the environmentally friendly road de-icer.[23] Furthermore, the dehydrogenation of formic acid can proceed easily under mild conditions.[24] Therefore, as an excellent hydrogen storage carrier, formic acid can play an important role in the future context of a hydrogen energy economic picture.

Although previous research has demonstrated the potential of the autocatalytic reduction of $CO_2$ into formic acid with zero-valent metal Fe under hydrothermal conditions, few studies have been focused on investigating the comprehensive pathways and reaction kinetics in $CO_2$ reduction. In this work, the detection and distribution for all products from the autocatalytic hydrothermal reduction of $CO_2$ were conducted, and then, based on these results, a possible reaction network and a quantitative model for the kinetics of hydrothermal carbon dioxide reduction were developed. Considering that $HCO_3^-$ is the product of $CO_2$ captured from waste streams by

Received: January 8, 2021
Accepted: April 8, 2021
Published: April 23, 2021

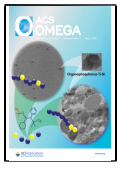

basic solution, $NaHCO_3$ was used as the $CO_2$ source. Simultaneously, the application of $NaHCO_3$ can also simplify the experimental procedure and ensure the accuracy of carbon amount.

## 2. RESULTS AND DISCUSSION

**2.1. Product Distribution.** First, a series of experiments were conducted to investigate the distribution of products from the reduction of $NaHCO_3$ in water with Fe as a reductant. From Figure 1, it was shown that formic acid was

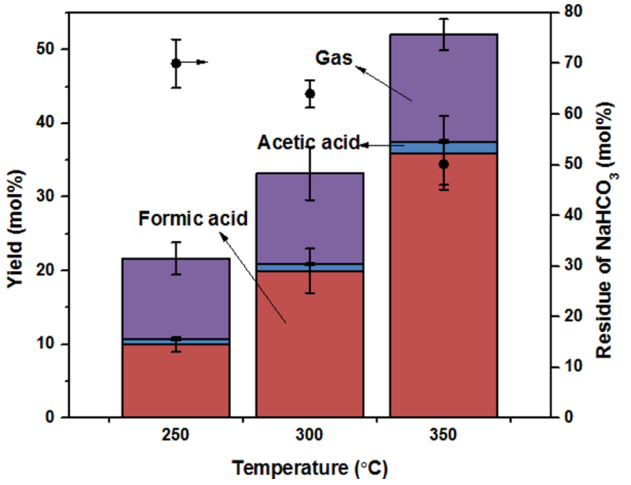


**Figure 1.** Distribution of products from hydrothermal reduction of $HCO_3^-$ (2 mmol $NaHCO_3$, 12 mmol Fe, and 600 s).

the main liquid product. A little amount of acetic acid was also detected after 600 s of reaction time. With the increase of the temperature, the conversion of $HCO_3^-$ significantly increased from 30 to 50 mol %, similarly with the trend for the yield of formic acid. However, the yields of gas products remained steady without significant change.

The analysis of the gas samples by gas chromatography/thermal conductivity detection (GC/TCD) showed that $H_2$, $CO_2$ and a trace amount of CO were produced at a reaction retention time of 600 s. In Table 1, it is obviously seen that the

**Table 1. Gas Product Distribution from Hydrothermal Reduction of $HCO_3^-$ at Different Temperatures (2 mmol $NaHCO_3$, 12 mmol Fe, and 600 s)**

| temperature (°C) | $H_2$ (wt %) | $CO_2$ (wt %) | CO (wt %) |
|---|---|---|---|
| 250 | 90 | 9.1 | 0.9 |
| 300 | 91 | 7.9 | 1.1 |
| 350 | 91 | 8.4 | 0.6 |

hydrogen was the main product in gas products, which was mainly from the decomposition of $H_2O$. Only a trace amount of CO was produced after the reaction. With the increasing temperature, the ratio of carbon dioxide was first decreased and then increased, which means that the decomposition of products such as formic acid and acetic acid appeared at higher temperatures.

**2.2. Effect of Reaction Time and Temperature.** A series of experiments were carried out to investigate the effect of residual time and temperature on hydrothermal conversion of $HCO_3^-$ by varying the time from 0 to 600 s and the reaction temperature from 250 to 350 °C with the same amount of Fe (12 mmol), respectively. As shown in Figure 2a, it was suggested that the yield of formic acid has shown a rapid increase with the increase of reaction time in 180 s at 250 and 300 °C, while the yield of formic acid increased linearly further with the reaction time over 300 s in all test temperatures. For the temperature at 350 °C, the yield of formic acid increased rapidly at all set reaction times. However, the trend of acetic acid yield was in contrast to that of formic acid. In Figure 2b, it was observed that the yield of acetic acid increased first from 0 to 600 s and dropped a little in 600 s at 350 °C. With regard to the decomposition of acetic acid, the decarboxylation pathway existed under hydrothermal conditions.[25] It has also been reported that acetic acid decomposed preferentially into $CO_2$ and $H_2$ at a temperature of 325 °C and a pressure of 350 bars.[26] The possible reason for the decreasing yield of acetic acid is that the decarboxylation of acetic acid dominated gradually and exceeded the formation rate of acetic acid with increasing temperature.

**2.3. Effect of the Fe Amount.** To further examine the effect of the hydrogen amount on the yield of product distribution, the effect of the initial Fe amount was also investigated at 350 °C. In Figure 3, it is shown that the yield of formic acid, acetic acid, and gas products all improved in the set reaction time (600 s) with the increase of the amount of Fe from 2 to 12 mmol. The high formic acid yield can be obtained without adding any other catalysts, which may be caused by several factors. First, being a closed system, when the $H_2$ amount was increased, the total gas amount and pressure increased; this caused the increase of $H_2$ partial pressure and the solubility of $H_2$ in the liquid phase. If the $H_2$ concentration was increased, the reaction rate of $HCOO^-$ also increased as per Le Chatelier's principle. The same effect can be achieved by increasing the pressure by reducing the empty volume of the reactor, which was shown by Roman-Gonzalez et al.[27] The second reason may be that $Fe_3O_4$ formed in hydrothermal conditions acted as a catalyst, which corresponds to the previous study.[28] In Section 3.2, it is also suggested that with the increase of temperature, Fe improved the formation of formic acid. It is possible that higher temperatures are favorable for the formation of $Fe_3O_4$.

To test this assumption, the X-ray diffraction (XRD) patterns of the solid residues obtained at different temperatures are shown in Figure 4. In our previous research, we indicated that Fe first reacts with $CO_2$ and $H_2O$ to form $FeCO_3$, which then loses $CO_2$ to form $Fe_3O_4$. In addition, the existence of $HCO_3^-$ also accelerated the Fe oxidation in water to produce hydrogen. Simultaneously, $Fe_3O_4$ is reduced in situ, leading to the formation of more active sites on the surface of $Fe_3O_{4-x}$.[28] The formed hydrogen and $HCO_3^-$ are activated on the $Fe_3O_{4-x}$ surface. This suggested that the more the Fe is oxidized to $Fe_3O_4$ under hydrothermal conditions, the more the surface of $Fe_3O_{4-x}$ and the amount of $H_2$ could be acquired, improving the reduction of $HCO_3^-$.

**2.4. Kinetic Modeling for the Hydrothermal Reduction of $HCO_3^-$.** Based on the above experimental data, the reaction network for hydrothermal reduction of $HCO_3^-$ was investigated in the present work, which differs from that offered recently for isothermal hydrothermal reduction of bicarbonate concentration at subcritical temperatures.[29] In Figure 5, the reaction network is proposed, which includes a primary pathway which shows that the reversible reaction appeared between bicarbonate concentrate and formate, a secondary pathway through two stages of tandem reaction for


https://doi.org/10.1021/acsomega.1c00119
ACS Omega 2021, 6, 11280−11285

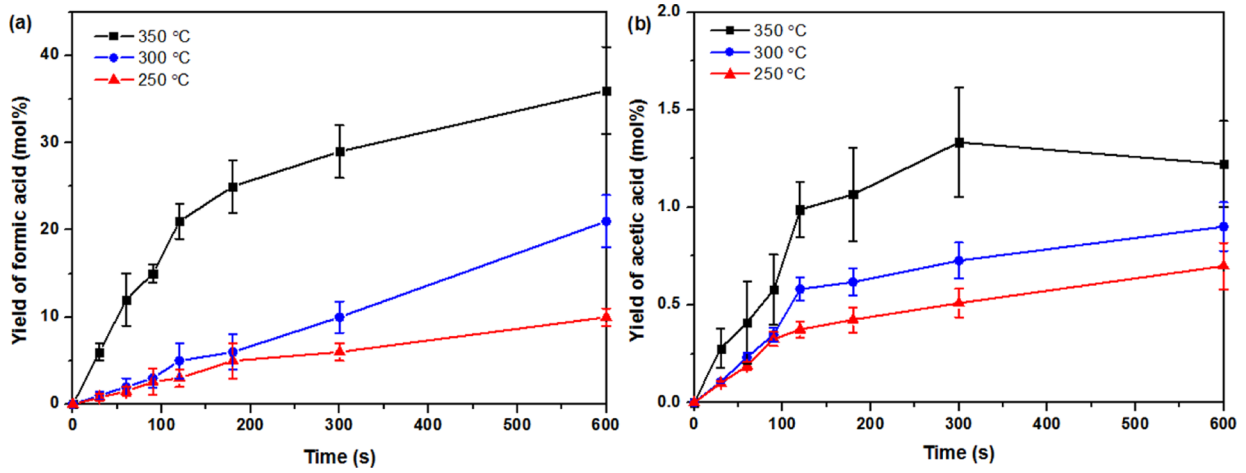


**Figure 2.** Effect of the reaction time and temperature on the yield of (a) formic acid and (b) acetic acid (2 mmol $NaHCO_3$, 12 mmol Fe and 600 s).

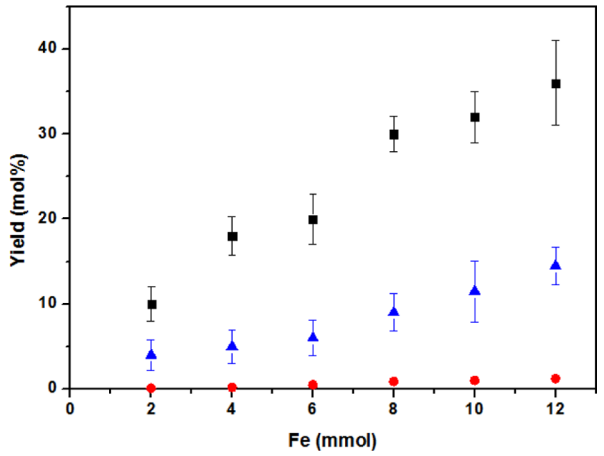


**Figure 3.** Effect of Fe amount on the hydrothermal reduction of $HCO_3^-$ at 350 °C for 600 s (■ formic acid, blue ▲ gas products, and red ● acetic acid).

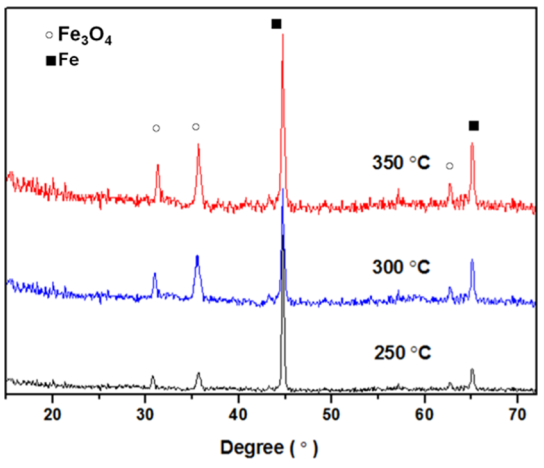


**Figure 4.** XRD patterns of the solid residues obtained at different temperatures.

the conversion of bicarbonate into acetate, and the final pathway that allows for gas formation from bicarbonate, formate, and acetate.

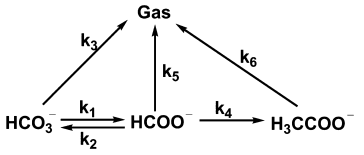


**Figure 5.** Reaction network for the hydrothermal reduction of $CO_2$.

Mathematica 10.2 was employed to solve the system of ordinary differential equations and simultaneously estimate the $A_i$ (Arrhenius pre-exponential factors) and $E_i$ (activation energies) of hydrothermal $HCO_3^-$ reduction by minimizing the sum of squared residuals (SSR) as eq 1.[30]

$$\mathrm{SSR} = \sum_i \sum_t (x_i(t) - x_{i,\mathrm{m}}(t))^2 \quad (1)$$

The first-order-rate law was postulated to describe the kinetics for each pathway, which corresponded with Chiang et al.[31] and then coupled them with the batch reactor design equation, as shown below in eqs 5−8. The subscripts on each mass fraction, $x_i$ and $k_i$, referred to the yields of each product fraction and the rate constants for pathways (liquids = $HCO_3^-$, FA = formic acid, AA = acetic acid, G = gas). The temperature profiles of the proxy reactors for each set point temperature were fitted using power series models and incorporated directly into the model to give the reactor temperature as a function of time. Additionally, we have assumed that all reactions take place in a single fluid phase.

$$\frac{dx_s}{dt} = -(k_1 + k_3 - k_2)x_s \quad (2)$$

$$\frac{dx_{FA}}{dt} = k_1 x_s - (k_2 + k_4 + k_5)x_{FA} \quad (3)$$

$$\frac{dx_{AA}}{dt} = k_4 x_{FA} - k_6 x_{AA} \quad (4)$$

$$\frac{dx_G}{dt} = k_3 x_s + k_5 x_{FA} + k_6 x_{AA} \quad (5)$$

In Table 2, we describe the kinetics parameters and optimized Arrhenius parameters for the hydrothermal reduction of $HCO_3^-$. It was determined that the activation energy for formation of formic acid from $HCO_3^-$ during


https://doi.org/10.1021/acsomega.1c00119
ACS Omega 2021, 6, 11280−11285

**Table 2. Arrhenius Parameters for the Hydrothermal Reduction of $HCO_3^-$**

| rate constant | pathway | $k_{250°C}$ ($min^{-1}$) | $k_{300°C}$ ($min^{-1}$) | $k_{350°C}$ ($min^{-1}$) | ln $A$ | $E_i$ (kJ/mol) |
|---|---|---|---|---|---|---|
| $k_1$ | liquids → formic acid | 0.00817 | 0.0143 | 0.0230 | 1.63 | 28 |
| $k_2$ | formic acid → solids | 0.00290 | 0.00657 | 0.0131 | 3.58 | 41 |
| $k_3$ | liquids → gas | 0.00022 | 0.000859 | 0.00269 | 7.21 | 68 |
| $k_4$ | formic acid → acetic acid | $7.04 \times 10^{-6}$ | $2.98 \times 10^{-5}$ | 0.0001 | 4.69 | 72 |
| $k_5$ | formic acid → gas | $3.08 \times 10^{-7}$ | $1.84 \times 10^{-6}$ | $8.22 \times 10^{-6}$ | 5.47 | 89 |
| $k_6$ | acetic acid → gas | $1.12 \times 10^{-9}$ | $9.76 \times 10^{-9}$ | $6.02 \times 10^{-8}$ | 4.22 | 108 |

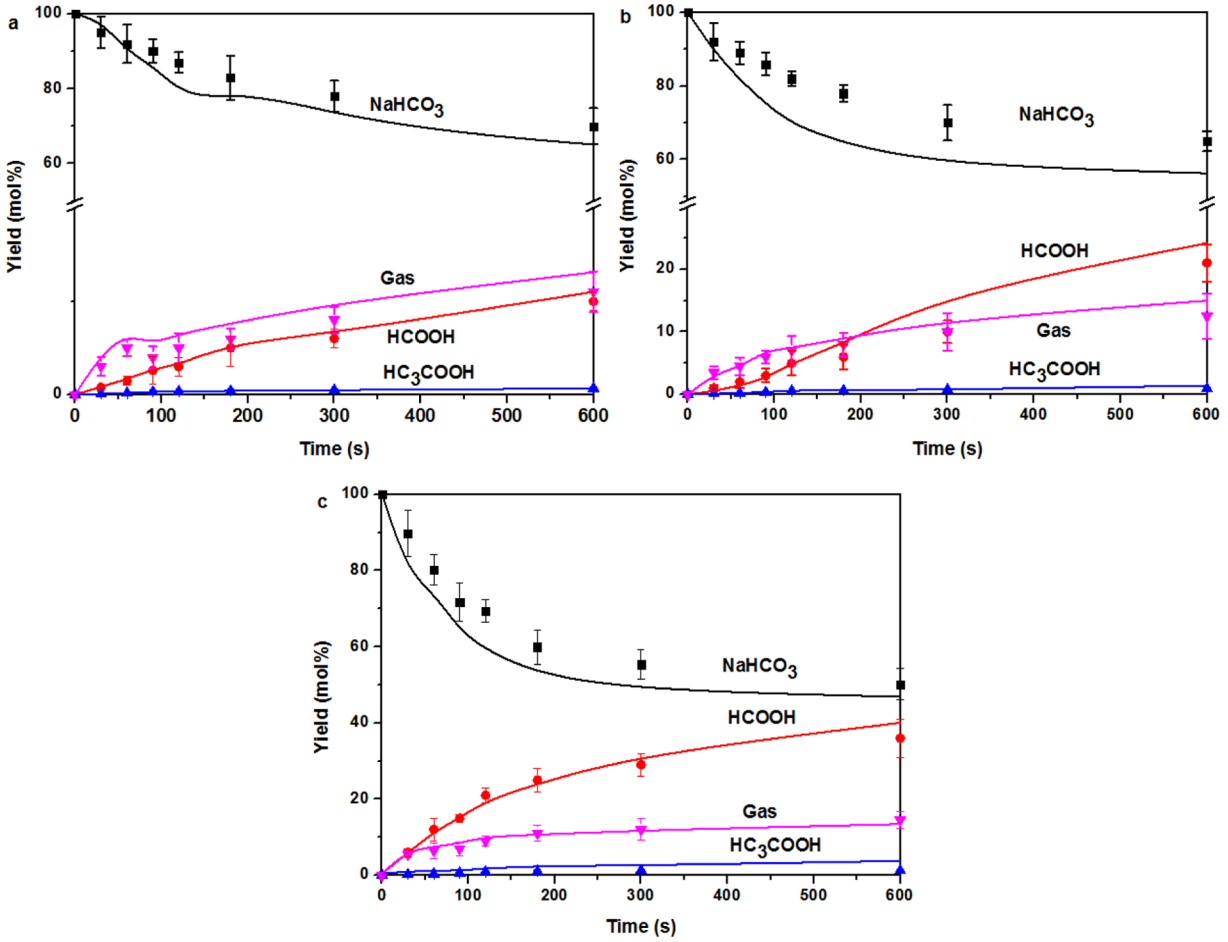


**Figure 6.** Experimental (points) and model calculated yields (continuous curves) for the hydrothermal reduction of $HCO_3^-$ at set point temperatures (a) 250, (b) 300, and (c) 350 °C with different reaction times (0−600 s).

hydrothermal conditions is about 28 kJ/mol, which is similar with the results from the range determined previously for decomposition of acids.[32] It was indicated that the kinetic constant for formic acid is significantly increasing with the temperature, which is consistent with the results from our experiments. The earlier kinetics modeling work on conventional hydrogenation of $CO_2$ provided an opportunity for comparison of these activation energies (80 kJ/mol), which are higher than our results from hydrothermal reduction.[33] However, the activation energy of acetic acid from formic acid is about 72 kJ/mol, which is the rate-determining step to limit the formation of acetic acid. The activation energies for the gasification of acetic acid are also comparable to activation energies reported by Belsky et al. for the decarboxylation of acetic acid and its derivatives (71−178 kJ/mol).[34]

According to the determined the kinetic parameters based on the results of experiments, the correlation between the model calculations and the experimental data for the hydrothermal reduction of $HCO_3^-$ at different temperatures and times are displayed in Figure 6. The model accurately describes the trends in the data and provides the species concentrations within experimental errors. From Figure 6a−c, it was also illustrated that the proposed reaction network and optimized Arrhenius parameters could capture the trends in the observed product yields for all three set point temperatures, which is also consistent with the first-order-rate law as postulated.

We also compared the yield of each product from experiment and the yield data from the predicted model in Figure 7. It displays a plot that compares the experimental and predicted product yields, in which the circles represent data from temperatures with long reaction time (0−20 min), triangles represent data from the amount of 14 mmol Fe, and squares represent data from 275 °C. It has been shown that the predicted data are almost below the diagonal. Though our perfection may not be fitted together to predict the product


https://doi.org/10.1021/acsomega.1c00119
ACS Omega 2021, 6, 11280−11285

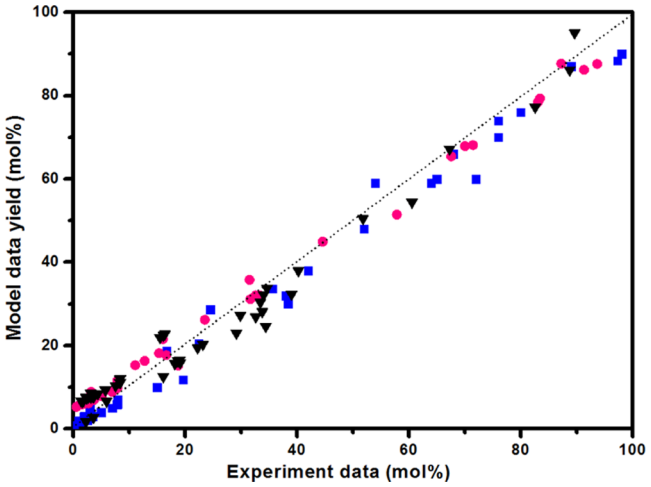


**Figure 7.** Parity plot for product fraction yields from fast reduction of $CO_2$. Circles represent data from the temperature with a long reaction time (0−20 min). Triangles represent data from the amount of 14 mmol Fe. Squares represent data from 275 °C.

yields from reduction of $CO_2$, it was a true prediction to an extrapolation to a reaction regime with limited parametrization.

## 3. EXPERIMENTAL SECTION

**3.1. Materials.** Zero-valence metal Fe powders (325-mesh size) were obtained from Aladdin Chemical Reagent, and $NaHCO_3$ (used as a $CO_2$ source) was obtained from Sinopharm Chemical Reagent Co., Ltd. All other reagents were commercially available from Sinopharm Chemical Reagent Co. Ltd. Deionized water was used throughout the study. The reactions were conducted by 316 stainless-steel Swagelok tube fittings with an internal volume of approximately 5.7 mL.

**3.2. Reactors and Hydrothermal Reduction Procedure.** In a typical experimental procedure, the desired amount of $NaHCO_3$ (2 mmol), Fe powder, and deionized water was loaded in a batch reactor to occupy 35% of the total reactor volume. After loading, the reactor was immersed in a salt bath, which has been preheated at the set point temperatures of 250, 300, and 350 °C. It took the time at which the reactor reached its isothermal temperature as $t$ = 0. While the reactors remained in the salt bath for an additional 0−600 s, the reactors were removed from the salt bath and cooled in a cold-water bath to quench the reactions. Then, the gas products were initially collected into a TCD for analysis, and the liquid and solid samples were separated through the filter membrane (0.22 $\mu$m filter film) for analysis, respectively. Liquid samples were analyzed by high-performance liquid chromatography (HPLC) (Agilent Technologies 1200 system), GC−flame ionization detector/mass spectrometry (Agilent 6890 gas chromatographs with a mass spectrometric), and a total organic carbon (TOC) analyzer (Shimadzu TOC 5000A). Solid residues were analyzed by XRD (Bruker D8 Advance X-ray diffractometer). All the experiments were conducted three times to force the influence of systematic errors.

Quantitative estimation of formic acid and acetic acid was based on the average value from the HPLC analysis, which was analyzed by the HPLC analyzer equipped with two Shodex RSpak KC-811 columns in series and a refractive index detector. The mobile solvent of the HPLC was $HClO_4$ (2 mmol/L) on a flow rate of 1.0 mL/min and holding 30 min. The yield of acids was defined as the percentage of formic acid or acetic acid and the initial $NaHCO_3$ on a carbon basis as follows in eqs 6, 7

$$Y_{FA} = \frac{C_{FA}}{C_S} \times 100 \text{ mol \%} \tag{6}$$

$$Y_{AA} = \frac{2C_{AA}}{C_S} \times 100 \text{ mol \%} \tag{7}$$

where $C_{FA}$, $C_{AA}$, and $C_S$ are the amounts of carbon in formic acid, acetic acid, and the initial $NaHCO_3$ added to the reactors.

For gas products, a 15 ft stainless steel column, as Carboxen 1000 (Supelco), was employed to separate each component in the gas phase sample, which used Ar as the carrier gas (15 mL/min). The programmed temperature of the column was first held at 40 °C for 5 min, followed by heating at a rate of 20 °C/min until it reached 220 °C and held for 10 min, which has a total of 24 min for the run time. To quantify the amount of gas, the high-pressure valve of the reactor was connected to a sampling valve attached to an Agilent Technologies model 6890N GC equipped with a TCD. The calibration curve relates the mole fraction, $y_i$, and the peak area for each component. The molar yield, $n_i$, of each component was subsequently calculated from the mole fractions of each compound detected in the gas chromatograph using eq 8, which was determined by the moles of $N_2$ from air in the reactor using the ideal gas law.

$$n_i = \frac{y_i}{y_{N_2}} \times n_{N_2} \tag{8}$$

## 4. CONCLUSIONS

In this work, a kinetic study was conducted for the first time to investigate the distribution of products from the autocatalytic hydrothermal reduction of $HCO_3^-$ using zero-valent metal Fe, and the pathways were proposed. The rate constants, activation energy, and frequency factors were calculated according to the Arrhenius equation, which is consistent with the first-order-rate law as postulated. The activation energy for the formation of formic acid from $HCO_3^-$ reduction is about 28 kJ/mol, which is much lower than that in the earlier kinetic modeling work on conventional hydrogenation of $CO_2$. The present study is helpful for providing a promising perspective to show the pathways and phenomenological kinetics of hydrothermal reduction of carbon dioxide.

## AUTHOR INFORMATION

### Corresponding Author

**Ligang Luo** − *College of Life Sciences, Shanghai Normal University, Shanghai 200240, China;* orcid.org/0000-0002-1405-7177; Email: ligangluo@shnu.edu.cn

### Authors

**Binbin Jin** − *School of Environmental Science and Engineering, Shanghai Jiao Tong University, Shanghai 200240, China*

**Longfei Xie** − *College of Chemistry and Molecular Engineering, East China Normal University, Shanghai 200241, China*

Complete contact information is available at: https://pubs.acs.org/10.1021/acsomega.1c00119



https://doi.org/10.1021/acsomega.1c00119
*ACS Omega* 2021, 6, 11280−11285

### Author Contributions

The article was written through the contributions of all authors. All authors have approved the final version of the manuscript.

### Notes

The authors declare no competing financial interest.

## ■ ACKNOWLEDGMENTS

The authors thank the financial support of the National Natural Science Foundation of China (grant no. 31801321), the Shanghai Sailing Program (grant no. 19YF1436300), and the Natural Science Foundation of Shanghai (grant no. 18ZR1428100).

## ■ REFERENCES

(1) Li, K.; An, X.; Park, K. H.; Khraisheh, M.; Tang, J. A critical review of $CO_2$ photoconversion: Catalysts and reactors. *Catal. Today* **2014**, *224*, 3−12.

(2) Huber, G. W.; Shabaker, J. W.; Dumesic, J. A. Raney Ni-Sn catalyst for $H_2$ production from biomass-derived hydrocarbons. *Science* **2003**, *300*, 2075−2077.

(3) Lal, R. Sequestration of atmospheric $CO_2$ in global carbon pools. *Energy Environ. Sci.* **2008**, *1*, 86−100.

(4) Aresta, M.; Dibenedetto, A. The contribution of the utilization option to reducing the $CO_2$ atmospheric loading: research needed to overcome existing barriers for a full exploitation of the potential of the $CO_2$ use. *Catal. Today* **2004**, *98*, 455−462.

(5) Hoffert, M. I.; Covey, C. Deriving global climate sensitivity from palaeoclimate reconstructions. *Nature* **1992**, *360*, 573−576.

(6) Hoffert, M. I.; Caldeira, K.; Benford, G.; Criswell, D. R.; Green, C.; Herzog, H.; Jain, A. K.; Kheshgi, H. S.; Lackner, K. S.; Lewis, J. S.; Lightfoot, H. D.; Manheimer, W.; Mankins, J. C.; Mauel, M. E.; Perkins, L. J.; Schlesinger, M. E.; Volk, T.; Wigley, T. M. L. Advanced technology paths to global climate stability: energy for a greenhouse planet. *Science* **2002**, *298*, 981−987.

(7) He, R.; Hu, B.; Zhong, H.; Jin, F.; Fan, J.; Hu, Y. H.; Jing, Z. Reduction of $CO_2$ with $H_2S$ in a simulated deep-sea hydrothermal vent system. *Chem. Commun.* **2019**, *55*, 1056−1059.

(8) Omae, I. Aspects of carbon dioxide utilization. *Catal. Today* **2006**, *115*, 33−52.

(9) Sahibzada, M.; Chadwick, D.; Metcalfe, I. S. Hydrogenation of carbon dioxide to methanol over palladium-promoted Cu/ZnO/$Al_2O_3$ catalysts. *Catal. Today* **1996**, *29*, 367−372.

(10) Borodko, Y.; Somorjai, G. A. Catalytic hydrogenation of carbon oxides−a 10-year perspective. *Appl. Catal., A* **1999**, *186*, 355−362.

(11) Tominaga, H.; Nagai, M. Density functional study of carbon dioxide hydrogenation on molybdenum carbide and metal. *Appl. Catal., A* **2005**, *282*, 5−13.

(12) Inui, T.; Kitagawa, K.; Takeguchi, T.; Hagiwara, T.; Makino, Y. Hydrogenation of carbon dioxide to C1-C7 hydrocarbons via methanol on composite catalysts. *Appl. Catal., A* **1993**, *94*, 31−44.

(13) Nam, S.-S.; Kim, H.; Kishan, G.; Choi, M.-J.; Lee, K.-W. Catalytic conversion of carbon dioxide into hydrocarbons over iron supported on alkali ion-exchanged Y-zeolite catalysts. *Appl. Catal., A* **1999**, *179*, 155−163.

(14) Jessop, P. G.; Leitner, W. *Chemical Synthesis Using Supercritical Fluids*; Wiley-VCH, 1999; p 358.

(15) Horita, J.; Berndt, M. E. Abiogenic methane formation and isotopic fractionation under hydrothermal conditions. *Science* **1999**, *285*, 1055−1057.

(16) McCollom, T. M.; Seewald, J. S. A reassessment of the potential for reduction of dissolved $CO_2$ to hydrocarbons during serpentinization of olivine. *Geochim. Cosmochim. Acta* **2001**, *65*, 3769−3778.

(17) Takahashi, H.; Liu, L. H.; Yashiro, Y.; Ioku, K.; Bignall, G.; Yamasaki, N.; Kori, T. $CO_2$ reduction using hydrothermal method for the selective formation of organic compounds. *J. Mater. Sci.* **2006**, *41*, 1585−1589.

(18) Fu, Q.; Sherwood Lollar, B.; Horita, J.; Lacrampe-Couloume, G.; Seyfried, W. E. Abiotic formation of hydrocarbons under hydrothermal conditions: Constraints from chemical and isotope data. *Geochim. Cosmochim. Acta* **2007**, *71*, 1982−1998.

(19) Wu, B.; Gao, Y.; Jin, F.; Cao, J.; Du, Y.; Zhang, Y. Catalytic conversion of $NaHCO_3$ into formic acid in mild hydrothermal conditions for $CO_2$ utilization. *Catal. Today* **2009**, *148*, 405−410.

(20) Lyu, L.; Zeng, X.; Yun, J.; Wei, F.; Jin, F. No Catalyst Addition and Highly Efficient Dissociation of $H_2O$ for the Reduction of $CO_2$ to Formic Acid with Mn. *Environ. Sci. Technol.* **2014**, *48*, 6003−6009.

(21) Jin, F.; Moriya, T.; Enomoto, H. Oxidation reaction of high molecular weight carboxylic acids in supercritical water. *Environ. Sci. Technol.* **2003**, *37*, 3220−3231.

(22) Jin, F.; Gao, Y.; Jin, Y.; Zhang, Y.; Cao, J.; Wei, Z.; Smith, R. L., Jr. High-yield reduction of carbon dioxide into formic acid by zero-valent metal/metal oxide redox cycles. *Energy Environ. Sci.* **2011**, *4*, 881−884.

(23) Kang, P.; Zhang, S.; Meyer, T. J.; Brookhart, M. Rapid selective electrocatalytic reduction of carbon dioxide to formate by an iridium pincer catalyst immobilized on carbon nanotube electrodes. *Angew. Chem., Int. Ed.* **2014**, *53*, 8709−8713.

(24) Tedsree, K.; Li, T.; Jones, S.; Chan, C. W. A.; Yu, K. M. K.; Bagot, P. A. J.; Marquis, E. A.; Smith, G. D. W.; Tsang, S. C. E. Hydrogen production from formic acid decomposition at room temperature using a Ag−Pd core−shell nanocatalyst. *Nat. Nanotechnol.* **2011**, *6*, 302−307.

(25) Watanabe, M.; Inomata, H.; Smith, R. L., Jr.; Arai, K. Catalytic decarboxylation of acetic acid with zirconia catalyst in supercritical water. *Appl. Catal., A* **2001**, *219*, 149−156.

(26) Bang, S. S.; Johnston, D. Environmental Effects of Sodium Acetate/Formate Deicer, Ice Shear. *Arch. Environ. Contam. Toxicol.* **1998**, *35*, 580−587.

(27) Roman-Gonzalez, D.; Moro, A.; Burgoa, F.; Pérez, E.; Nieto-Márquez, A.; Martín, Á.; Bermejo, M. D. 2Hydrothermal $CO_2$ conversion using zinc as reductant: Batch reaction, modeling and parametric analysis of the process. *J. Supercrit. Fluids* **2018**, *140*, 320−328.

(28) Duo, J.; Jin, F.; Wang, Y.; Zhong, H.; Lyu, L.; Yao, G.; Huo, Z. $NaHCO_3$-enhanced hydrogen production from water with Fe and in situ highly efficient and autocatalytic $NaHCO_3$ reduction into formic acid. *Chem. Commun.* **2016**, *52*, 3316−3319.

(29) Zhong, H.; Yao, H.; Duo, J.; Yao, G.; Jin, F. Pd/C-catalyzed reduction of $NaHCO_3$ into $CH_3COOH$ with water as a hydrogen source. *Catal. Today* **2016**, *274*, 28−34.

(30) Luo, L.; Sheehan, J. D.; Dai, L.; Savage, P. E. Products and kinetics for isothermal hydrothermal liquefaction of soy protein concentrate. *ACS Sustainable Chem. Eng.* **2016**, *4*, 2725−2733.

(31) Chiang, C.-L.; Lin, K.-S.; Chuang, H.-W. Direct synthesis of formic acid via $CO_2$ hydrogenation over Cu/ZnO/$Al_2O_3$ catalyst Author links open overlay panel Journal of Cleaner Production. *J. Cleaner Prod.* **2018**, *172*, 1957−1977.

(32) Yu, J.; Savage, P. E. Decomposition of formic acid under hydrothermal conditions. *Ind. Eng. Chem. Res.* **1998**, *37*, 2−10.

(33) Suh, H.-W.; Schmeier, T. J.; Hazari, N.; Kemp, R. A.; Takase, M. K. Experimental and Computational Studies of the Reaction of Carbon Dioxide with Pincer-Supported Nickel and Palladium Hydrides. *Organometallics* **2012**, *31*, 8225−8236.

(34) Belsky, A. J.; Maiella, P. G.; Brill, T. B. Spectroscopy of Hydrothermal Reactions 13. Kinetics and Mechanisms of Decarboxylation of Acetic Acid Derivatives at 100−260 °C under 275 bar. *J. Phys. Chem. A* **1999**, *103*, 4253−4260.



https://doi.org/10.1021/acsomega.1c00119
*ACS Omega* 2021, 6, 11280−11285